From Spectral Holeburning Memory to Spatial-Spectral Microwave Signal Processing

Wm. Randall Babbitt[1,2,*], Zeb W. Barber[1], Scott H. Bekker[2], Michael D. Chase[2], Calvin Harrington[1], Kristian D. Merkel[2], R. Krishna Mohan[1], Tia Sharpe[1], Colton R. Stiffler[2], Aaron S. Traxinger[2], and Alex J. Woidtke[2]

[1] Spectrum lab, Montana State University, Bozeman, MT – 59717-3510

[2] S2 Corporation, Bozeman, Montana 59715

*Corresponding author: babbitt@physics.montana.edu

Abstract

Many storage and processing systems based on spectral holeburning have been proposed that access the broad bandwidth and high dynamic range of spatial-spectral materials, but only recently have practical systems been developed that rival the performance and capabilities of electronic devices. This paper reviews the history of the proposed applications of spectral holeburning and spatial-spectral materials from frequency domain optical memory to microwave photonic signal processing systems. The recent results of a 20 GHz bandwidth high performance spectrum monitoring system with the additional capability of broadband direction finding demonstrate the potential for spatial-spectral systems to be the practical choice for solving demanding signal processing problems in the near future.

Introduction

The ability to use spectral holeburning (SHB) techniques to store high volume frequency domain information in spatial-spectral (S2) materials was recognized over 30 years ago.[1] Memory devices based on frequency domain [2] and time-domain [3] were some of the first proposed applications. Over the past 30 years, many time-domain signal processing applications based on SHB have been proposed and demonstrated. Initial demonstrations were typically in the MHz regime, and some were later extended to the processing or creation of GHz signals.[4,5,6,7] In 2002, the concept of using S2 materials to process microwave signals by storing the correlation of microwave signals in the S2 material and then reading out the result through a scan of the absorption profile was introduced.[8] The first proposed application was correlative radar processing,[9] but subsequent applications included spectral analysis,[10,11,12,13] noise lidar,[14] time-integrating correlators,[15] squint-free imagers,[16] radar direction finding,[17] and analog to digital conversion.[18] This paper gives a historical perspective of the advancement from spectral holeburning as a potential memory device to the currently operating and field tested broadband (over 20 GHz) spatial spectral spectrum analyzers.

Background on Microwave Signal Processing and Spectral Readout in S2 materials

Frequency-Domain Spectral Holeburning

The main feature of S2 materials is their ability to respond selectively to a broad range of frequency inputs. S2 materials can have frequency selectivity down to 100Hz,[19] and store or process bandwidths over a THz [20], yielding a high frequency domain dynamic range. The large number of accessible ions at each frequency enable high signal dynamic range. These attributes coupled with spatial and angular multiplexing capabilities [16] make S2 materials an attractive medium for high volume storage and process applications. The frequency selectivity or resolution of an S2 material is limited to the materials homogeneous linewidth, $\delta\omega_h$. The range of continuous frequencies that a S2 material can store or process is limited by its inhomogeneous linewidth, $\delta\omega_i$. For microwave signal processing applications, materials with homogeneous linewidth less than a MHz and inhomogeneous linewidth on the order of 10-200GHz are typically used. These include Er:LiNbNO3, Tm:LiNbNO3, Tm:YAG, and Tm:YLuAG [19]. When a narrow band laser illuminated a S2 material, it burns a spectral hole only at the laser frequency with a width that is the convolution of the laser linewidth and the homogeneous linewidth. To store multiple holes, the laser can be tuned across the inhomogeneous profile and potentially a million holes can be recorded, which is the basis for the frequency domain optical memories proposed in the 1970's.[2] If the laser beam is spatially modulated, holograms of a large set of images can be stored at each frequency location.[20] The recall of the frequency domain memory information or a particular spectral holograms is achieved by tuning a laser to the appropriate frequency and reading out the absorptive feature or hologram. By scanning the laser across the inhomogeneous profile, multiple bits of information or images are read out in series. Frequency domain memory and hologram storage represent the first cases of frequency domain readout of information stored in S2 materials.

Time-Domain Spectral Holeburning

A temporally modulated optical signal can be decomposed into multiple frequency components. If the modulated signal illuminates a S2 material, the individual components burn separate spectral holes into the absorption profile of the S2 material. Assuming the components are not strong enough to saturate the absorption at any frequency, the spectral structure burned into the absorption profile will be proportional to the power spectrum of the input signal. If E(t) is the input signal and $E(\omega)$ its Fourier transform, the modified absorption profile (to first order in the power spectrum) is $\alpha(\omega)L=\alpha_0 L-\beta|E(\omega)|^2$, where β is a material constant. If the signal is longer the $T_2=\pi/\delta\omega_h$, the homogeneous coherence lifetime of the material, the burned power spectrum is convolved with $\delta\omega_h$. If E(t) is shorter than T_2 and consists of the two sequential signals, $E_1(t)$ and $E_2(t-t_{21})$, delayed by t_{21} from one another, the combined power spectrum is

$$\left|E(\omega)\right|^2=\left|E_1(\omega)\right|^2+\left|E_2(\omega)\right|^2+\left(E_1^*(\omega)E_2(\omega)\exp(i\omega t_{21})+c.c.\right)$$

The cross terms is on a "spectral" carrier and thus is distinguishable from the individual power spectrums. One way to distinguish the spectral hologram of the two signals is by applying a

third pulse, $E_3(t-t_3)$, at time t_3, that generates a temporal output signal (provided distortion effects, like those introduced by possible hyperfine structure can be ignored [21])

$$E_{echo}(t) = \int d\omega E_1^*(\omega) E_2(\omega) E_3(\omega) \exp\left(i\omega\left(t - t_3 - t_{21}\right)\right)$$

This result can be used for time-domain memory [3] if two of the three pulses are reference signal or signal processing applications. The product of Fourier Transforms in the frequency domain results in the output representing the convolution and/or correlation of the input pulses. The first two pulses can also be long (>>T2) chirped pulses and either angled or delayed with respect to each other by less than T_2. The results can be used for TTD [22] or rainbow spectrometer [23].

Frequency-Domain Readout of Processed Temporal Information

Drawbacks of performing microwave signal processing via the full bandwidth temporal readout of the modified absorption spectrum is the need for fast detectors and signal to noise considerations due to the microwave to optical to microwave conversion and the low efficiency (<<10%) of the stimulated photon echo process. In 2002, the first frequency-domain readout of SHB-based microwave signal processing was performed in a S2 material.[8] The signal processing operation was the correlation of the transmit and receive radar signals, one delayed from the other. The long population lifetime in S2 materials allowed the accumulation of several signal pulse pairs to build up the modified absorption spectrum, which was then read out with a slow (much longer than T_2) optical chirp. The detected signal when Fourier Transformed reveals the delay and thus the range to the target. Multiple discrete targets with different ranges could be simultaneously sensed. Demonstrations of radar processing with S2 materials were carried out, with operational bandwidths up to 2 GHz..[9]

Spectrum Analysis in S2 Materials

One powerful processing application of S2 materials is simply spectral analysis of a broadband microwave signal. This was first suggested in a paper in 2003 [24] and demonstrated in 2004 by collaborations between groups in Colorado, Montana, and France [25,26,27]. (In 2004, it was also suggested and demonstrated that S2 materials could be used to create hyper-spectral images of the sun [20]). Initially, it was thought that the readout time of a spectrum from an absorption profile was limited by the desired resolution bandwidth of the spectrum analyzer, limiting the chirp rate, κ, to $(\delta\omega_{res})^2$ [25, 27, 28]. Readout faster than this rate causes distortion of the spectral hole, due to Kramers-Kronig relation [20]. Consequently, each hole produces a ringout response that lasts for the reciprocal of the hole width, spectrally spreading each hole in bandwidth by $\kappa/\delta\omega_{res}$ [29]. For example, 0.1 MHz resolution would require a chirp rate of less than 0.01 (MHz/μs). If this were true, reading out 10 GHz of spectra would require over a second, longer than the population decay times of the S2 materials used, as well as longer than desired update rates for practical applications.

However, provided the chirped laser is coherently phase stable (other than quadratic phase evolution of chirps), the transmitted intensity of the output signal represents a linear impulse

response to the features of the modified absorption profile. In 2005, a post-detection recovery algorithm was developed to undue the ring out induced distortions.[30] Figure 1 shows the ring out in the detected signal due to a sharp spectral feature (top curves of each set) and the result of the post-processing the signal with a recovery algorithm (bottom curve of each set). The limit on the spectral resolution of the recovered spectral feature is governed by the bandwidth, δf_{det}, of the detector and digitizer used to capture the transmitted output from the chirped readout of the S2 material. The achievable resolution is $\kappa/\delta f_{det}$, enabling fast high dynamic range recovery of stored spectra. In practice, this translates into being able to readout a 10 GHz spectrum with 0.1 MHz resolution in about 1 ms with a detector-digitizer bandwidth of 100MHz, which is 1000 times faster than the readout rate of $(\delta\omega_{res})^2$ when not using recovery.

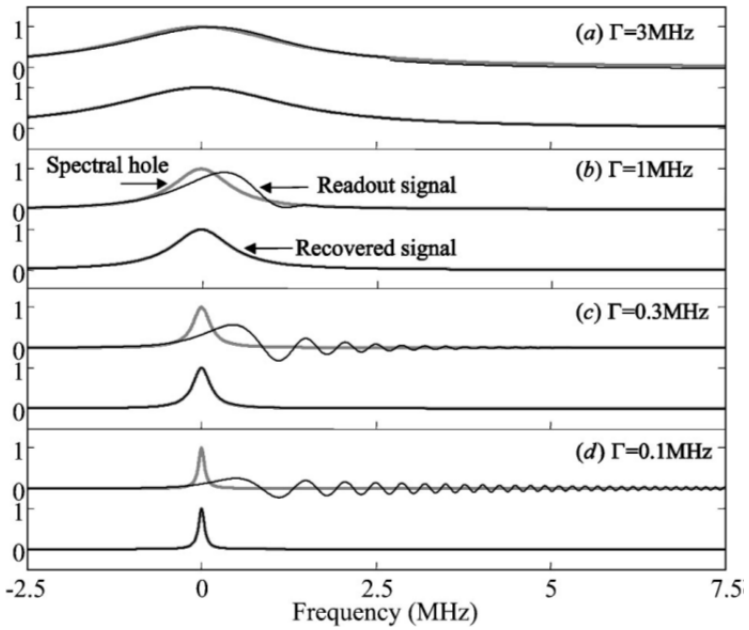

Figure 1 Simulations of chirped readout (k =1 MHz/ms) of spectral holes of various widths. The normalized readout and recovered signals are plotted as a function of frequency for comparison with the normalized spectral hole. The recovery processing uses the readout data with a band width from −10 to 10 MHz. To show the details of the signal, the frequency scale in the plot is from −2.5 to 7.5 MHz.[30]

S2 Spectrum Analyzer

The current development of the spatial-spectral spectrum analyzer (S2 SA) based on chirped readout is driven towards high performance and field testing. At the S2 SA's core is a small crystalline sample (~1 cm^3) of Tm:YAG maintained at 4K in a commercial cryo-refrigerator with custom vibrational isolation of the crystal. The Tm:YAG has an inhomogeneous linewidth of about 17 GHz and an inhomogeneous linewidth at 4 K of about 10 KHz. [19] With an upper state lifetime of 0.8 msec and bottleneck lifetime of 10 msec,[19] Tm:YAG makes a good integrator and short term memory for spectrum analysis. The major challenge of the S2 SA is to convert microwave signals-of-interest (SOIs) from the electronic domain to the optical domain with minimal distortion and with sufficient power (at full RF power) to burn deep holes in the S2 material. In our tests of the S2 SA, SOIs are collected via wideband antennas as well as coupled directly into the S2 SA input. The microwave signals are typically amplified before driving an

electro-optic waveguide phase modulator, which transfers the SOI's microwave power spectrum as sidebands onto a low phase noise, frequency stable laser. One sideband of the modulated light is resonant with the 793 nm absorbing optical transition of Tm:YAG burning the SOI's power spectrum into the crystal absorption profile. The ions within each homogeneous linewidth integrate the energy incident at that frequency that arrives within the bottleneck lifetime. Once recorded, the modified absorption spectrum is stored in the S2 material for several milliseconds giving sufficient time for a stable optical chirp to scan across the absorption spectrum. Readout chirp durations can be a varied from > 1 ms to as short as 5 μs, generating spectral frame rates of 1-200 kHz. The transmission of the readout chirp through the crystal generates a modulated output signal. The resultant output signal is balanced detected using the response from a second spot in the crystal that was not illuminated by the SOI. The balanced signal is recorded at 250 MSPS and digitally post-processed to remove residual background. Spectral recovery is applied to extract an accurate microwave spectrum from the distorted response from the fast optical chirp caused by the narrow spectral features burned into the crystal.

The current S2 SA system is capable of hours of continuous spectral measurement including streaming the data to disk. In a recent demonstration of the S2 SA, over 100 seconds of dynamic microwave spectral activity over 20GHz bandwidth was continuously captured at a 5 kHz spectral frame rate. The optical readout chirp rate was 40 MHz/μs. Each spectral frame is stored to disk and can be analyzed separately, or combined via averaging or max hold operations for real-time display or detailed analysis of the spectral activity. The 20 GHz spectrum shown in the top of Figure 2 is the 'max-hold' over 40 spectral frames, where the maximum signal in each frequency bin over a 20 msec time period is used as the value for that frequency bin. At the bottom of Figure 1, these 'max–hold' spectra were converted to a color mapped spectrogram over a continuous 24 second period (120 'max-hold' spectral frames) to help display all the spectral activity during that period. The recording starts at the bottom of the spectrogram and ends at the top, with the 'max-hold' spectrum at the top of the figure representing the latest 'max-hold' spectrum recorded. The dynamic microwave environment was created using a variety of signal generators with internal and external modulation, as well as sources captured via antenna, such as cell phones, microwave ovens, Bluetooth, and Wi-Fi. For example, a microwave carrier with multiple side tones in the 15-20 GHz range was pulsed on and off for a while and then jumped to the 10-15 GHz range at approximately the 80th 'max-hold' frame. A signal generator that was frequency stepped from 12-18GHz was given variable broadband sidebands via mixing with a random digital waveform on a carrier. Another signal generator produced single tone bursts from a random frequency list starting in the 5-10 GHz range around the 50th 'max-hold' frame, which then later hopped to the 1-6 GHz range. It is an important feature of the S2 SA, that all of the microwave activity during the capture was captured by the S2 material and integrated into its modified absorption spectrum. This 100% probability of detection of incoming signals is in contrast with spectrum analyzers based on scanning filters or digitizer, which miss all signals that are not within a narrow band around the instantaneous frequency of the scanner. A 100 MHz measurement bandwidth real-time spectrum analyzer when scanning out a 20 GHz spectrum misses 99.5% of the incoming signals.

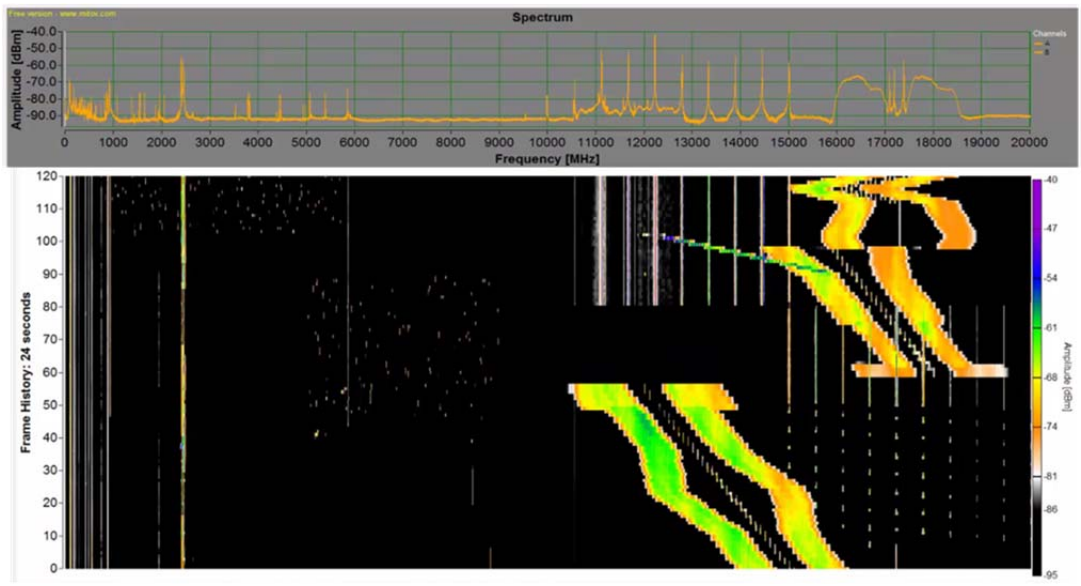

Figure 2 Demonstration of continuous spectral monitoring over 20 GHz bandwidth of a dynamic microwave environment with the S2 SA.

The data recorded was also examined with zoomed in spectrograms, showing the 0.2 msec temporal resolution, 0.25 MHz pixel spacing, and <1 MHz 3dB spectral resolution of each recorded frame. Three zoomed spectrograms are shown in Figure 3. The left zoomed spectrogram tracks the evolution a modulated frequency hopped source over 2.25 second in a band that extends from 5.3 GHz to 9.2 GHz. The microwave carrier starts off steady at 6.88GHz, while the 0.7 GHz sidebands are square wave modulated at 75MHz. First the sideband carrier frequency is slightly reduced, and then the carrier is stepped up in frequency. The S2 SA tracks the carrier and sidebands throughout these dynamics. At the same time, a narrow band cw source (just visible in top left of spectrogram) is also tracked, with a measured linewidth of less than 1 MHz. The middle zoomed spectrogram shows a 100 MHz wide by 330 msec long zoomed spectrogram of Wi-Fi (the broader features) and Bluetooth (the narrower pulses features) sharing the same spectrum in the ISM band around 2.5 GHz. The top right zoomed spectrogram shows 130 MHz wide by 75 msec long study of a frequency hopping synthesizer that is having trouble locking onto its assigned frequency around 3.21 GHz. The bottom right zoomed spectrogram is zoomed to 12 MHz wide by 7 msec into the start of the tone on the left in spectrogram above it, showing the slide of the synthesizer's frequency of about 7 MHz for 2 msec (with 0.2msec resolution) before it arrives at its assigned frequency. It should be note that the synthesizer does not typically have this problem at most frequencies (though at least 5 other such slides were observed during a quick surf through the spectrograms). This error would not easily be detected with the tracking capabilities of the S2 SA, especially if you were trying to tracking a randomly hopping unknown source. It should be emphasized that the 20 GHz wide and 12 MHz wide spectrograms all come from the same data set captured at 5 kHz frame rate.[31]

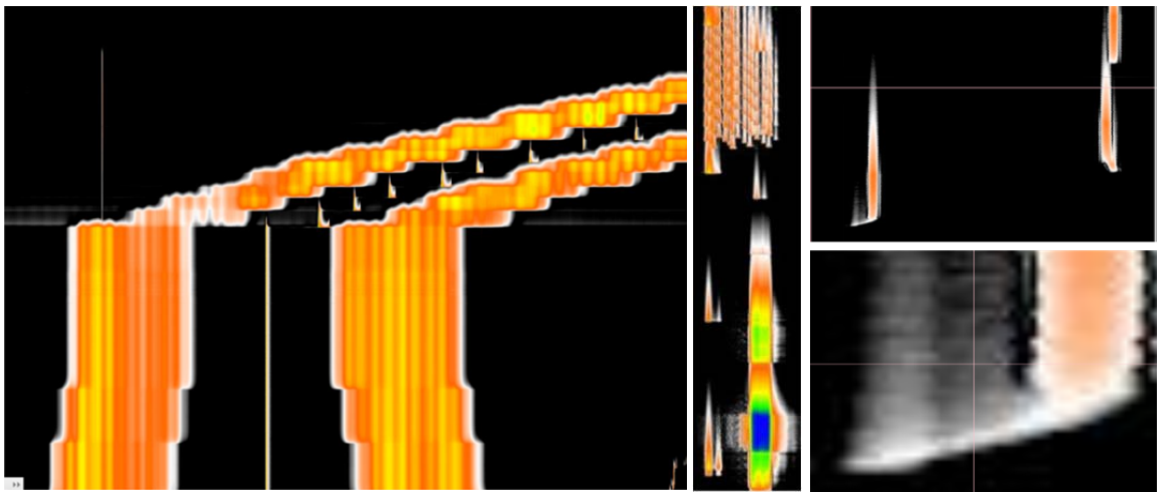

Figure 3 Demonstration of ability to zoom into 20 GHz wide 120 second long captured data to monitor activity with sub-MHz spectral resolution and 0.2 msec temporal resolution. The right zoomed spectrogram is a 2.25 sec long by 3.9 GHz wide tracking of a modulated frequency hopping source. The middle is a 100 MHz wide by 330 msec long zoomed spectrogram showing Bluetooth (top) and Wi-Fi (broad channels on bottom) sharing the ISM band around 2.5GHz. The top right is a The top right is a 130 MHz wide by 75 msec long zoomed spectrogram studying the turn-on characteristic of a frequency hopping synthesizer around 3.21 GHz. The bottom right 12 MHz by 7 msec zoomed spectrogram shows the synthesizer's frequency sliding 7 MHz for 2 msec (with 0.2msec resolution) before locking onto its assigned frequency.

A critical specification for spectral monitoring devices is its spur free dynamic range (SFDR). The SFDR is typically measured by inputting two frequency tones (f_1 and f_2), which are varied together in power as the third order intermodulation distortion tones at $2f_1$-f_2 and $2f_2$-f_1 are monitored. An interesting feature of S2 SA is that the material intrinsically has a very high SFDR, since multiple tones that are absorbed by the crystal do not produce new frequencies (intermodulation products). This is due to the nonlinearity of the crystal occurring in the frequency domain and not the time domain. Unlike most microwave systems, where saturation of the device usually signals the onset of distortion, S2 materials saturate without creating frequency domain distortion, other than the saturation of the peak. The SFDR of the S2 SA system is not limited by the S2 material, but instead by the devices used to amplify the microwave and optical signals before the crystal and the electro-optic conversion.

The SFDR of the S2 SA was measured by tracking the third order tones produced by tones at 5.0 and 5.5 GHz as the powers of the tones were varied together, as shown in inset in Figure 4. The noise level was recorded in a frequency region away from the two tones. The SFDR results are plotted in Figure 4 for two different sensitivity settings of the S2 SA. The plots show the initial linear rise of the main tones and saturation, which occur at rf power at least 20 dB lower than the onset of the TOI tones, demonstrating that the S2 material itself does not limit the SFDR. For the low sensitivity setting (no gain on the microwave signal) the SFDR was measured to be 63dB. The minimum detected cw signal for this setting was -65dBm and the third order intercept point (IP3) was 30dBm. In a higher sensitivity setting with 58 dB of gain, the minimum detectable cw signal improved to -123 dBm, an IP3 of -31dBm, and a slight drop in SFDR to 62 dB. Further adjustments of the laser power and gain enabled an -133dBm minimum detection signal level (in 1 MHz), but at the expense of dropping the SFDR to 53 dB.

Methods to obtain further improvements in the sensitivity and SFDR of the S2 SA are currently under development, however the S2 SA's SFDR is already 6 dB to 16 dB higher than the fastest state-of-the-art commercial digitizer (the 12.5 Gigasample per second Tektronix TADC-1000), which only has 6 GHz of bandwidth and a SFDR of 47 dB.[32]

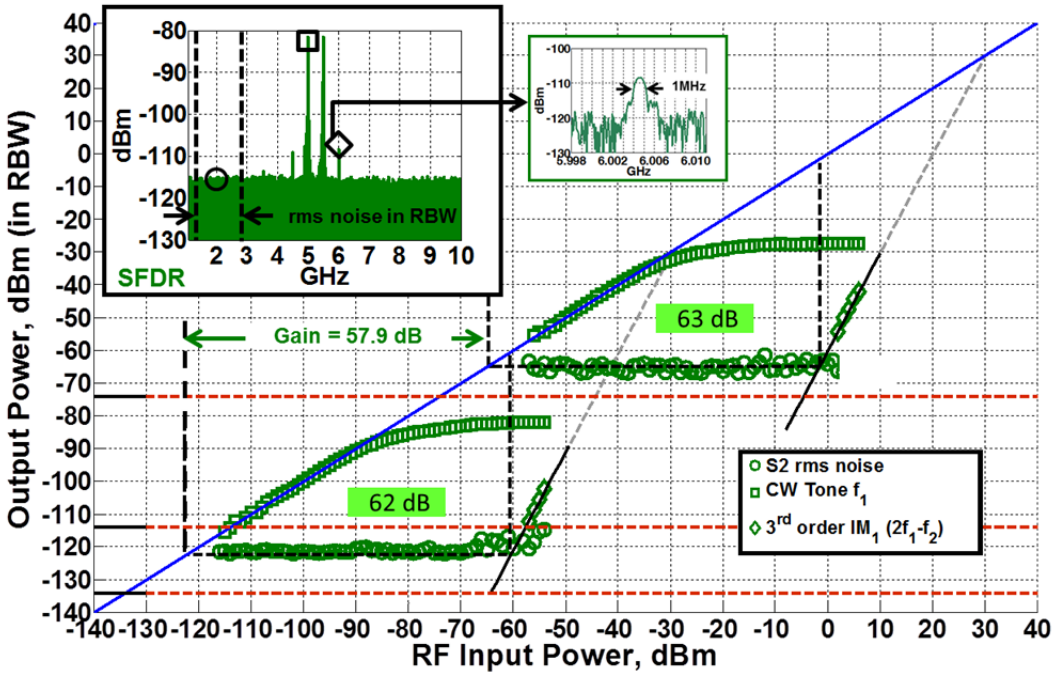

Figure 4 Measurements that demonstrate the S2 SA system's high SFDR of 63 dB.

S2 Spectrum Analysis and Direction Finding

The ability of the S2 SA to make simultaneous measurements of microwave power in each resolvable frequency bin and to multiplex the measurement of more than one antenna in a single crystal enable the S2 SA to be extended to also measuring the direction of arrival of the microwave power in a two or more antenna system. Phase sensitive direction finding (DF) systems rely on measuring the relative time delay in reception of passive radio signals between two or more antennas to make a determination of the direction of the radio emitter. A variety of techniques for processing the antenna signals to obtain DF information have been developed [33], including several microwave DF systems based on photonic processing [34,35,36]. Phase sampled linear interferometry is a well-known RF and microwave DF approach that utilizes known antenna element spacing and the phase relationships between detected signals to estimate the angle of arrival (AoA) of an emitter [37].

The S2 SA/DF system uses a RF-optical interferometric technique as an analog pre-processor of the signals from two antennas before they are recorded by a 2-channel S2 spectrum analyzer. The two-element antenna concept is presented in Figure 5. In this configuration the SOI received by the two antenna elements has a time difference of arrival (TDOA) that

depends on the SOI's AoA θ, given by $\tau = (d/c)\sin(\theta)$, where c is the speed of light and d is the antenna element spacing. If the time-shifted signals from the two elements drive the two electro-optic phase modulators (EOPM) in a dual-drive quad-biased Mach-Zehnder interferometer (MZI) device, there will be a differential splitting of the optical power at each frequency into the two output ports of the MZI. The two output ports of the interferometer will thus have different optical power spectra. The optical spectra of the two ports can be measured accurately with fine resolution over a broad bandwidth with a dual-channel S2 SA. The sum of the two spectra yields the microwave power spectrum of the incident SOIs. The ratio of the sum and difference of the two spectra at any given frequency can be used to determine the relative phase (delay) at every frequency and thus the AoAs of incident SOIs.

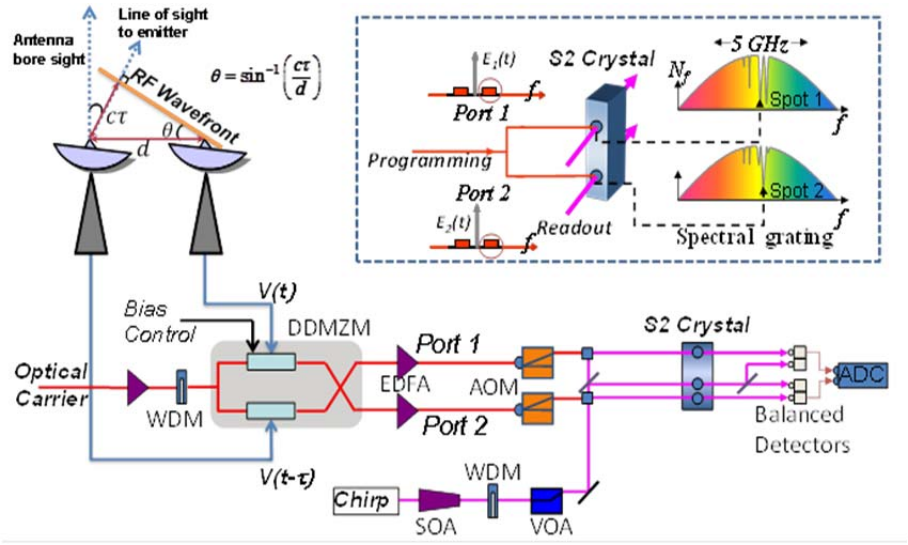

Figure 5 The S2 DF system. Mock antenna signals with variable delays were generated and drove the two port of the DDMZM. In the demonstration the readout chirp beam was counter-propagating to the programming beams. EDFA: Erbium doped fiber amplifier; SOA: Semiconductor optical amplifier; VOA: Variable optical attenuator; WDM: Wavelength Division Multiplexing filter. The amplified and gated outputs from the two ports of the DDMZM are programmed into two spatial spots in a S2 material, as shown in inset.

The theory for the S2 DF system presented here is similar to that of the dual-drive, single-port, dual-sideband, version of the S2 DF system that used a single channel S2 SA to measure both optical sidebands around the optical carrier [38]. The single-port dual-sideband approach suffers from operational limitations. Only one half (at most) of the operational bandwidth of the S2 crystal can be utilized in the single port system since both optical sidebands must be analyzed. In addition, to avoid spurious 2nd harmonic signals, the frequency coverage of optical readout needs to be four times the SOI bandwidth (for sub-octave bandwidth signals). For the two-port output MZI in Figure 5, if the dual-drive, dual-port MZI modulator (DDMZM) is operated at quadrature bias, then the output spectra of the two ports will be 'mirror' images of each other, with the upper sideband of the one port will be identical to the lower sideband of the other and vice versa. Thus, if either both upper sidebands or both lower sidebands of the two ports are readout, the power spectra and phase information needed to

estimate the power spectrum and the time difference of arrival of the SOI is available. For the two-port configuration, the readout chirp bandwidth required is only a function of the bandwidth being analyzed, in contrast to the single-port S2 DF.

The analysis is the same for the cases of recording and reading out either the upper (U) or lower (L) sideband of the two output ports. The power spectra in upper sidebands of ports 1 and 2, $P_{1U}(\omega)$ and $P_{2U}(\omega)$, are proportional to the SOI power spectrum, but modulated by $[1 \pm \sin(\omega\tau(\omega))]$, where $\tau(\omega)$ is the delay between the signals from the two antennas at angular frequency $\omega = 2\pi f$. Thus, the sum of the two ports spectra yields the microwave (when converted appropriately) spectrum of the SOI. Taking the ratio of the difference and sum of the port's spectra yields

$$S(\omega) = \frac{P_{1U}(\omega) - P_{2U}(\omega)}{P_{1U}(\omega) + P_{2U}(\omega)} = \sin(\omega\tau(\omega))$$

The time delay at each resolvable frequency component over a broad bandwidth can then be extracted using$\tau(\omega) = \sin^{-1}\big(S(\omega)\big)$.

The inset in Figure 5 illustrates how the desired sideband (upper or lower) can be positioned at the most optically responsive center of the absorption band in contrast with the dual-sideband approach in reference [38], where the two sidebands were recorded in the wings of the absorption profile with the optical carrier positioned at the center, resulting in low sensitivity and reduced SNR. The S2 SA/DF system thus more readily enables broader band SA/DF on signals with carrier frequencies much greater than their bandwidth.

The system illustrated in Figure 5 was used to demonstrate the S2 SA DF operation. The S2 material was a 0.02%Er:2%Eu:YSO crystal (5mm x 17mm x 20mm, produced by Scientific Materials Inc.), which was held at 1.5 K in 0.3-0.5 T magnetic field. The Er:Eu:YSO has its absorption peak at 1536 nm with a width of 14 GHz.[19] The bias of the custom DDMZM (produced by EOSpace Inc.) was controlled to operate at quadrature ($\theta_{MZ} = \pm\pi/2$) using a YY Labs bias controller. The DDMZM was driven with two identical but time-delayed microwave signals. The time delays to be measured were introduced through mechanical line stretchers. Various microwave signals were synthesized and used as the desired SOIs. Each optical output of the DDMZM was amplified with a 1W Keopsys erbium doped fiber amplifier (EDFA). The amplified ports of the interferometer were incident on two spatial locations of the S2 material, gated by two acousto-optic modulators (AOMs). The programmed spectral gratings were read out for each time delay with a wideband optical chirp, which was amplified with a SOA and gated with a VOA. A collinear counter-propagating single pass optical geometry was exploited whereby the programming and readout optical paths traveled along the same axis but in opposite directions. Each readout channel was detected with a balanced detector. An additional readout path through the material was created to generate a reference input to balance each detector. A 16 bit 200 MS/s GaGe digitizer card was used to capture the outputs from the balanced detectors. The acquired readout spectra were post-processed to recover the spectra and yield the phase function that was then used to estimate the time delay at each frequency, $\tau(\omega)$. Balancing the response of the two ports is essential for accurate DF. The digitized output of port 2 had to be multiplied by 1.4 to maintain this balance. A variety

of waveforms, including tones, chirped waveforms, and modulated pulses were used to test the system performance. Additionally, signals with multiple SOIs with different delays were tested, demonstrating over 5 GHz of instantaneous bandwidth and multi-emitter tracking capability of the S2 DF system.

This S2 SA/DF system was tested with pure tones, frequency chirped (linear frequency modulated) pulses, and RF carriers modulated with pseudo-random sequences. The results for a microwave signal consisting of a 100 μs long pseudo-random sequence at 1.3 Gbits per second (Gbps) modulated onto a 3.8 GHz carrier are shown in Figure 6 and Figure 7. The upper graph in Figure 6 shows the measured power spectrum of the SOI (the sum of the spectra measured in the two ports). The time delay was analyzed over the central 0.8 GHz of the SOI's spectrum, where the power spectrum was relatively flat. The central portion of upper graph of Figure 6 shows the ten overlapping measured spectra for different delays, demonstrating the ability of the S2 DF to perform SA and DF simultaneously. Each spectrum, as well as the time delay plots in the lower graphs of Figure 6, results from the measurement of a single 100 microsecond waveform (no averaging of multiple events). The lower graph in Figure 6 shows the measured time delays in every 1 MHz spectral channel over 800 MHz of bandwidth (corresponding to 800 separate delay measurements of a single broadband waveform).

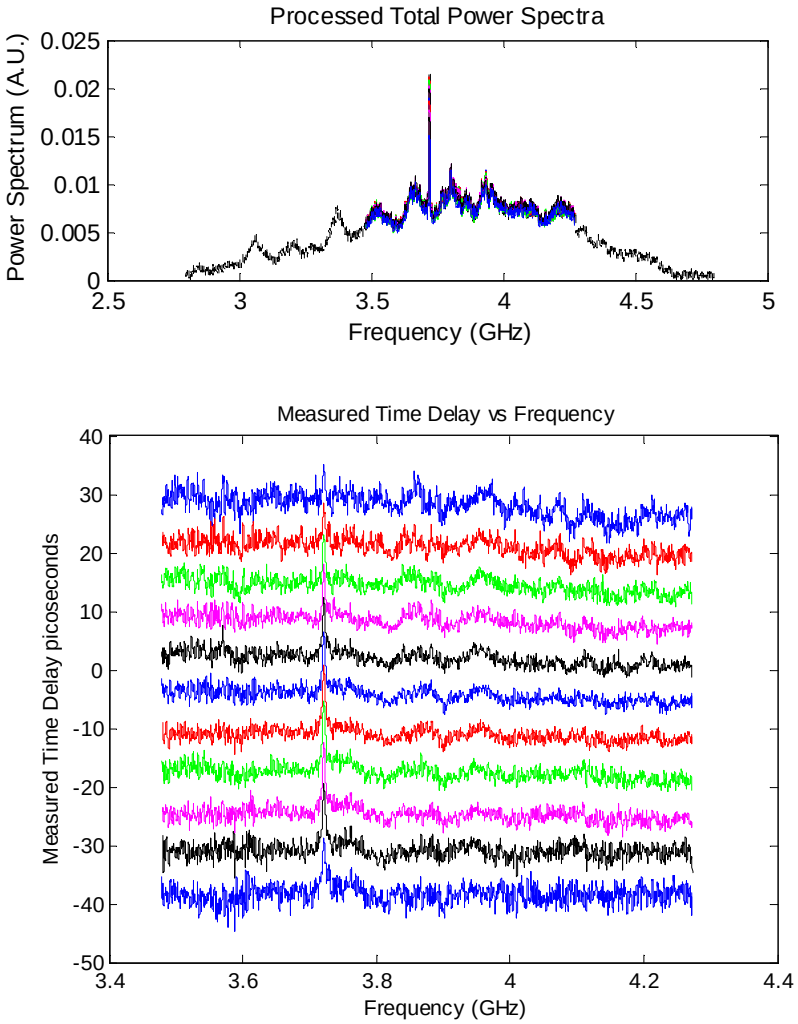

Figure 6 Power spectra (top) produced by summing the power spectra of the sidebands and time delay measurements (bottom) for a 1.3 Gbps pattern modulated onto a 3.8 GHz carrier with variable relative delays at the DDMZM input

Figure 7 shows measured mean delay estimated from the 800 delay measurements made for each programmed delay plotted against the programmed delays for separate measurements of the waveform for each delay. The same delay offset was added to all measured delays to align the two axes. The root mean square (RMS) deviation between the mean delay over the 800 MHz from the programmed delay was 0.5 ps. A formula for the RMS error (rms_τ) in the delay measurements was derived and is given by,

$$rms\_\tau = \frac{\sqrt{(3+\sin(2\omega\tau(\omega)))}}{\omega\cos(\omega\tau(\omega))SNR}$$

where the signal to noise (SNR) is the SNR of each 1MHz measurement of the summed power spectra, which was measured to be 18 dB. The lower graph in Figure 7 shows the single-shot RMS error over the 800 MHz bandwidth as a function of the programmed delay. The

theoretical curve shows the predicted RMS delay error for an 18 dB SNR. Systematic errors across the frequency band may be due to improper balancing of the MZI coupling, the RF drives, the bias of the DDMZM, and an imbalance in the measurement of the two ports. The RMS resolution of 1 ps at zero delay (on bore site) corresponds to a <0.5° angular resolution at 3.8 GHz for a λ/2 antenna spacing. The measured delays in this demonstration correspond to a ±15 degree field of view, but can be extended to a much larger field of view. Similar measurements were made on a 6.7 GHz waveform with delays of ±30 ps, corresponding to a ±25 degree field of view. The RMS error does increase away from zero delay.

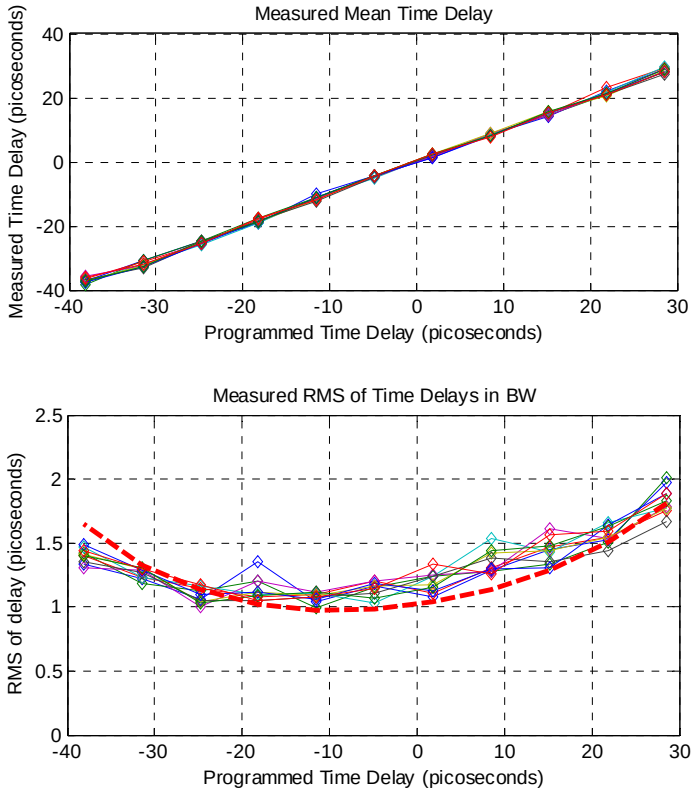

Figure 7 Top: Spectral mean of 10 measurements of the time delays for each programmed time delay. Bottom: RMS error of the individual time delays for different programmed delays and the theoretical curve for the expected RMS error in the delay measurement in a 1 MHz bandwidth. Both graphs include ten different applications of the SOIs.

The S2 SA/DF can handle multiple emitters from multiple directions (provided they have some spectral non-overlap for a two-element antenna array), and provides the direction and integrated power spectral density at every resolvable frequency component received, independent of the emitters' broadcast waveform type. Direct mapping of relative spectral phase and power spectra of RF signals received from a two-element antenna array can be performed, enabling high-spectral and high-angular resolution direction finding. The procedure can readily be expanded to arrays with additional antennas, utilizing the multiple spatial channels available in a single S2 crystal. Since the S2 DF measures the phase of incoming signal in each resolvable bandwidth, it works on all signals such as narrowband or broadband, sparse or dense, tones or modulated, and frequency chirped and frequency-hopped waveforms. The resolution of the delay measurements is independent of the SOI bandwidths. This attribute

can be contrasted with competing Fourier transform methods that rely on bandwidth to get precise time delay measurements. Multiple SOIs can be tracked simultaneously. The measurements are instantaneous, so the AoA and power spectrum can be determined for a single transient emission, even for signal durations much less than a millisecond. Finally, the S2 DF approach is also expandable to applications of advanced DF algorithms [33] and multi-element arrays for tracking spectrally and temporally overlapped emitters.

Summary

Many applications of SHB and S2 holography have been proposed and demonstrated. The recent demonstration of a broadband S2 spectrum analyzer that outperforms state-of-the-art commercial electronic systems and devices proves the practical advantage of SHB and S2 holography enhanced technology. This work opens the door to the development of other S2 material based systems for meeting the requirements of demanding, real-world signal processing applications.

Acknowledgment

The authors wish to acknowledge the funding support of the National Science Foundation (NSF) under the Small Business Technology Transition Research (STTR) program, effort 1217637. The results presented here are based on work supported by the Space and Naval Warfare Systems Center Pacific under contract No. N66001-09-C-2002. Any opinions, findings and conclusions or recommendations expressed in this material are those of the authors and do not necessarily reflect the views of the Space and Naval Warfare Systems Center Pacific.

References

[1] A. Szabo, U.S. Patent No. 3,896,420 (July 22, 1975); G. Castro, D. Haarer, R. M. MacFarlane, and H. P. Trammsdorff, U.S. Patent No. 4,101,976 (July 18, 1978); D. M. Burland, U.S. Patent No. 4,158,890 (June 19, 1979).

[2] C. Ortiz, R. M. MacFarlane, R. M. Shelby, W. Lenth, and G. C. Bjorklund, "Thin-Film Aggregate Color-Centers As Media For Frequency-Domain Optical Storage," Appl. Phys. 25,87 (1981).

[3] T. W. Mossberg, "Time-domain frequency-selective optical data storage," Opt. Lett. 7, 77 (1982)

[4] N. W. Carlson, L. J. Rothberg, A. G. Yodh, W. R. Babbitt, and T. W. Mossberg, "Storage and Time Reversal of Light Pulses Using Photon Echoes," Opt. Lett. 8, 483 (1983); Y. S. Bai, W. R. Babbitt, N. W. Carlson, and T. W. Mossberg, "Real-Time Optical Waveform Convolver/Cross Correlator," Appl. Phys. Lett. 45, 714 (1984). W. R. Babbitt and J. A. Bell, "Coherent Transient Continuous Optical Processor," Applied Optics, 33, 1538 (1994). C. J. Renner, R. R. Reibel, M. Tian, T. Chang, and W. R. Babbitt, "Broadband photonic arbitrary waveform generation based on spatial-spectral holographic materials," JOSA B, Vol. 24, 2979-2987 (2007).

[5] H. Sonajalg, A. Gorokhovskii, R. Kaarli, V. Palm, M. Ratsep, and P. Saari, "Optical pulse shaping by filters based on spectral hole burning," Opt. Commun. 71, 377–380 (1989).

[6] Heinrich Schwoerer, Daniel Erni, and Alexander Rebane, 'Holography in frequency-selective media. III. Spectral synthesis of arbitrary time-domain pulse shapes, J. Opt. Soc. Am. B, 12, 1083 (1995).

[7] X.A. Shen and R. Kachru, "Optical header recognition by spectroholographic filtering,"Opt. Lett. 20, 2508 (1995). X. A. Shen, R. Hartman, R. Kachru, "Impulse-equivalent time-domain optical memory," Opt. Lett. 21, 833 (1996).

[8] Z. Cole, T. Böttger, R. Krishna Mohan, R. Reibel, W. R. Babbitt, R. L. Cone and K. D. Merkel, "Coherent integration of 0.5 GHz spectral holograms at 1536 nm using dynamic biphase codes," Appl. Phys. Lett 81, 3525-3527 (2002).

[9] K.D. Merkel, R. Krishna Mohan, Z. Cole, T. Chang, A. Olson, and W. R. Babbitt, "Multi-Gigahertz radar range processing of baseband and RF carrier modulated signals in Tm:YAG," J. Lum. 107, 62-74 (2004). T. L. Harris, K. D. Merkel, R. K. Mohan, T. Chang, Z. Cole, A. Olson, and W. R. Babbitt, "Multigigahertz range-Doppler correlative signal processing in optical memory crystals," Applied Optics, 45(2), 343-352 (2006).

[10] L. Ménager, J.-L. Le Gouët, I. Lorgeré, Time to frequency Fourier transform with photon echoes, Opt. Lett. 26 1397 (2001).

[11] G. Gorju, V. Crozatier, I. Lorgeré, J.-L. Le Gouët, F. Bretenaker, 10-GHz bandwidth RF spectral analyzer with MHz resolution based on spectral hole burning in Tm3+:YAG, IEEE Photonics Technol. Lett. 17 2385–2387. (2005) G. Gorju, V. Crozatier, I. Lorgere, J.-L. Le Gouet, F. Bretenaker, "Wideband RF spectral analyzer based on spectral-spatial holography in Tm3+:YAG achieved with a highly stabilized frequency chirped laser, " J. Lum. 127, 110 (2007). G. Gorju, A. Chauve, V. Crozatier, I. Lorgeré, J.L. Le Gouët, and F. Bretenaker, "10 GHz Bandwidth rf spectral analyzer with megahertz resolution based on spectral–spatial

holography in Tm3+:YAG: experimental and theoretical study," J. Opt. Soc. Am. B 457 (2007).
[12] F. Schlottau, M. Colice, K. H. Wagner, and W. R. Babbitt, "Spectral hole burning for wideband, high-resolution radio-frequency spectrum analysis," Optics Letters, 30, 3003-5 (2005). R. Krishna Mohan, T. Chang, M. Tian, S. Bekker, A. Olson, C. Ostrander, A.Khallaayoun, C. Dollinger, W.R. Babbitt, Z. Cole, R.R. Reibel, K.D. Merkel, Y. Sun, R. L. Cone, F. Schlottau, K. H. Wagner, "Ultra-wideband spectral analysis using S2 technology," J. Lumin. 127, 116-128 (2007).
[13] J.L. Le Gouët, F. Bretenake, and I. Lorgeré, "Atomic Processing Of Optically Carried Rf Signals," Advances In Atomic, Molecular And Optical Physics, 54, 550 (2007).
[14] Y. Li, A. Hoskins, F. Schlottau, K. H. Wagner, C. Embry, and W. R. Babbitt, "Ultrawideband coherent noise lidar range-Doppler imaging and signal processing by use of spatial-spectral holography in inhomogeneously broadened absorbers," Applied Optics, 45, 6409-6420 (2006). Z. Cole, P. A. Roos, T. Berg, B. Kaylor, K. D. Merkel, W. R. Babbitt, and R.R. Reibel, "Unambiguous Range-Doppler LADAR processing using 2 giga-sample-per-second noise waveforms," J. Lumin. 127, 146-151 (2007).
[15] Friso Schlottau*, Kelvin H. Wagner, "Demonstration of a continuous scanner and time-integratingcorrelator using spatial–spectral holography," Journal of Luminescence 107, 90 (2004)
[16] B. M. Braker, F. Schlottau and K. Wagner, "Squint-Free Fourier-Optical RF Beamforming Using a SHB Crystal as an Imaging Detector," IEEE Select. Topics in Quan. Elect. 14, 952 (2008).
[17] Z. W. Barber, C. Harrington, C. W. Thiel, W. R. Babbitt, and R. Krishna Mohan, "Angle of Arrival Estimation Using Spectral Interferometry", J. Lum. 130, 1614-1618 (2010).
[18] W. R. Babbitt, M. A. Neifeld, and K. D. Merkel, " Broadband Analog to Digital Conversion with Spatial-Spectral Holography," J. Lumin. 127, 152-157 (2007). R. Reibel, C. Harrington, J. Dahl, C. Ostrander, P. Roos, T. Berg, R. Mohan, M. Neifeld, and W. R. Babbitt, "Demonstrations of analog-to-digital conversion using a frequency domain stretched processor," Optics Express 17, 11281-11286 (2009).
[19] C.W. Thiel, T. Böttger, and R.L. Cone, J. of Luminescence, 131, 3, 353–36 (2011).
[20] Alois Renn, Urs P. Wild, and Aleksander Rebane, "Multidimensional Holography by Persistent Spectral Hole Burning", J. Phys. Chem A 106, 3045 (2002).
[21] I.V. Yevseyev and V.A. Reshetov, "On The Influence Of The Resonant Level Hyperfine Structure On The Process Of Information Storage By Means Of Photon Echo," Optics Comm. 72, 377 (1989).
[22] K. D. Merkel and W. R. Babbitt, "Optical coherent transient true-time delay regenerator," Optics Letters 21, 1102-1104 (1996). K.D. Merkel, W.R. Babbitt, K.E. Anderson, and K.H. Wagner, "Variable-time delay optical coherent transient signal processing," Optics Letters, 24, 1386-1388 (1999). R. R. Reibel, Z. W. Barber, J. A. Fischer, M. Tian, and W. R. Babbitt, "Broadband demonstrations of true-time delay using linear sideband chirped programming and optical coherent transients," J. Lum. 107, 103-113 (2004).
[23] L. Ménager, I. Lorgeré, , J.-L. Le Gouët, D. Dolfi, J.-P. Huignard, "Demonstration of a radio-frequency spectrum analyzer based on spectral hole burning," Opt. Lett. 26, 1245 (2001). I. Lorgeré, L. Ménager, V. Lavielle, J.-L. Le Gouët , D. Dolfi, S. Tonda, J.-P. Huignard, Demonstration of a radio-frequency spectrum analyser based on spectral hole

burning, J. Mod. Opt. 49, 2459 (2002); V. Lavielle, I. Lorgeré, J.-L. Le Gouët, S. Tonda, D. Dolfi, Wideband versatile radio-frequency spectrum analyzer, Opt. Lett. 28 (2003) 384–386. ; V. Lavielle, F. De Seze, I. Lorgeré, J.-L. Le Gouët,Wideband radio frequency spectrum analyzer: improved design and experimental results, J. Lumin. 107, 75 (2004);

[24] F. Schlottau, K. Wagner, J. Bregman, and J.-L. Le Gouet, "Sparse antenna array multiple beamforming and spectral analysis using spatial-spectral holography,"IEEE Intl. Topical Meeting on Microwave Photonics, 355(2003).

[25] M. Colice, F. Schlottau, K. Wagner, R.K. Mohan, W.R. Babbitt,I. Lorgere, J.-L. Le Gouët, in Optical Information Systems II (SPIE Proc. 5557), ed. by B. Javidi, D. Psaltis, pp. 132–139 (October 2004)

[26] R.K. Mohan, Z. Cole, R.R. Reibel, T. Chang, K.D. Merkel, W.R. Babbitt, M. Colice, F. Schlottau, K.H. Wagner, "Microwave spectral analysis using optical spectral holeburning," in: Proc. Of Microwave Photonics (MWP), Ogunquit, MA, (October 2004).

[27] J.-L. Le Gouët, I. Lorgeré, F. Bretenaker, V. Lavielle, V. Crozatier, "Atomic spectral analyzers for radio frequency signals processing," in: "Proc. IEEE/LEOS Annual Meeting, Puerto-Rico", (October 2004).

[28] I. Lorgere, V. Crozatier, G. Gorju, F. Bretenaker, J.-L. Le Gouet, "Radio-frequency spectrum analyzers based on rare earth ion doped crystals," Appl. Phys. B 84, 653 (2006).

[29] T. Chang, R. K. Mohan, M. Tian, T. L. Harris, W. R. Babbitt, and K. D. Merkel, "Frequency-chirped readout of spatial-spectral absorption features," Phys. Rev. A. 70, 063803 (2004).

[30] T. Chang, M. Tian, R. K. Mohan, C. Renner, K. D. Merkel, and W. R. Babbitt, "Recovery of spectral features readout with frequency chirped laser fields," Opt. Lett. 30, 1129 (2005).

[31] The spectrograms shown in the figures in this paper are available on-line at s2corporation.com/public/Jan_2014/090-100s/ , with the capability to explore 120 seconds of captured data and zoom in and out from 12 MHz to 20 GHz wide spectrograms.

[32] TADC-1000 Data Sheet, http://component-solutions.tek.com/literature-library/TADC-1000%20Data%20Sheet%20-%20Tektronix%20Component%20Solutions%20-%20LR.pdf

[33] "Advances in Direction-of-Arrival Estimation," S. Chandran, ed., Artech House, Norwood, MA (2006)

[34] S. Tonda-Goldstein, D. Dolfi, A. Monsterleet, S. Formont, J. Chazelas, and J. P. Huignard, "Optical signal processing in radar systems," IEEE Trans. Microw. Theory Tech., 54,2, 847–853 (2006).

[35] B. Vidal, M. A. Piqueras, and J. Martí, "Direction-of-Arrival Estimation of Broadband Microwave Signals in Phased-Array Antennas Using Photonic Techniques," Journal of Lightwave Technology, Vol. 24, Issue 7, pp. 2741- (2006).

[36] X. Zou, W. Li, W. Pan, B. Luo, L. Yan, and J. Yao, "Photonic approach to the measurement of time-difference-of-arrival and angle-of-arrival of a microwave signal," Optics Letters, Vol. 37, Issue 4, pp. 755-757 (2012).

[37] P. Pace, High-Resolution Phase Sampled Interferometry Using symmetrical Number Systems, IEEE Transactions on Antennas and Propagation, 49, 10, 1411 (2001).

[38]Z. W. Barber, C. Harrington, C. W. Thiel, W. R. Babbitt, R. Krishna Mohan, Angle of arrival estimation using spectral interferometry, J Luminescence, vol. 130, no. 9, 1614-1618 (2010).